Research Article J. Electrochem. Sci. Technol., 2016, 7(4), 277-285

Journal of Electrochemical Science and Technology
jecst.org

An Electrochemical Sensor for Hydrazine Based on *In Situ* Grown Cobalt Hexacyanoferrate Nanostructured Film

Inhak Kang†, Woo-seung Shin†, Shanmugam Manivannan*, Yeji Seo, and Kyuwon Kim*
Electrochemistry Laboratory for Sensors & Energy (ELSE), Department of Chemistry, Incheon National University, Incheon 406-772, Republic of Korea

ABSTRACT

There is a growing demand for simple, cost-effective, and accurate analytical tools to determine the concentrations of biological and environmental compounds. In this study, a stable electroactive thin film of cobalt hexacyanoferrate (Cohcf) was prepared as an *in situ* chemical precipitant using electrostatic adsorption of Co^{2+} on a silicate sol-gel matrix (SSG)-modified indium tin oxide electrode pre-adsorbed with $[Fe(CN)_6]^{3-}$ ions. The modified electrode was characterized by scanning electron microscopy, X-ray diffraction, X-ray photoelectron spectroscopy, and electrochemical techniques. Electrocatalytic oxidation of hydrazine on the modified electrode was studied. An electrochemical sensor for hydrazine was constructed on the SSG-Cohcf-modified electrode. The oxidation peak currents showed a linear relationship with the hydrazine concentration. This study provides insight into the *in situ* growth and stability behavior of Cohcf nanostructures and has implications for the design and development of advanced electrode materials for fuel cells and sensor applications.

Keywords : Cobalt hexacyanoferrate, Electrocatalysis, Electrochemical sensor, Hydrazine, Sol-gel matrix

Received : 23 September 2016, Accepted : 10 October 2016

1. Introduction

Metal hexacyanoferrates are an important class of insoluble mixed-valence polynuclear compounds; they are widely used to prepare chemically modified electrodes [1,2] because they can produce well-characterized electroactive films with properties similar to those of redox and ion-exchange polymers [3,4]. The use of metal hexacyanoferrates in the form of thin films to enhance the interfacial properties of solid electrodes has been the focus of much interest over the past three decades [5,6]. Such thin solid films are widely used in many applications, such as electrochemical sensors, electrocatalysts, electrochromic display devices, and supercapacitors [7-11]. Furthermore, among various electron transfer mediators, metal hexacyanoferrates are preferred because their redox reactions can proceed without dissolution of the material, as the ion diffusion maintains charge balance inside the material. Cobalt hexacyanoferrate (Cohcf) is an analog of Prussian blue and is of particular interest owing to its electrochromic properties [11], reversible photo induced magnetization [12], and decent catalytic activity [13,14]. The redox processes of metal hexacyanoferrates are coupled with insertion and release of an alkali metal cation to ensure electro neutrality during the redox reaction [15]. In particular, Cohcf films are reportedly capable of showing cation (K^+, Na^+)-dependent electrochromic and thermochromic behavior, indicating that Cohcf is unique among metal hexacyanoferrates.

Environmental impacts caused by hydrazine (N_2H_4) accumulation and contaminations are significant concerns in terms of human health. Monitoring of variations in the concentration of N_2H_4 is essential to understanding its biogeochemical processes in aquatic environments and to developing better strate-

†Both authors contributed equally

*E-mail address: kyuwon_kim@inu.ac.kr
smanivannan1982@yahoo.com

DOI: https://doi.org/10.5229/JECST.2016.7.4.277

gies for water quality management, waste water treatment, and food industry processes. N_2H_4 is widely used as a starting material in the production of insecticides, herbicides, pesticides, dyestuffs, and explosives, as well as in the preparation of several pharmaceutical derivatives [16]. N_2H_4 is also an ideal fuel for direct fuel cell systems, as its electrooxidation process does not suffer from any poisoning effects [17-21]. In addition, the maximum recommended level of hydrazine in trade effluents is 1 ppm [22]; therefore, a sensitive method is required for its reliable measurement.

Here we present a stable electroactive thin solid film of Cohcf prepared using two-step electroless fabrication [23]. Electrostatic adsorption of Co^{2+} on an amine-functionalized silicate sol-gel matrix (SSG)-modified indium tin oxide (ITO) electrode pre-adsorbed with $[Fe(CN)_6]^{3-}$ ions was used to grow the *in situ* chemical precipitant Cohcf. The synthesis and stabilization of nanostructures (NSs) embedded in the SSG have the advantages of single-step preparation, uniform distribution of nanometer-sized particles, and versatility of matrix forms (sols, gels, films, and monoliths) [24]. The resulting films are conductive and inorganic; furthermore, an SSG possessing an active redox center makes them possible electrocatalysts toward oxidation of N_2H_4. In this approach, the amine functional groups of the SSG essentially serve as nucleation sites for *in situ* growth of Cohcf NSs. Moreover, this well-organized thin solid film of SSG-Cohcf demonstrates great potential for further applications in future photo magnetic devices, sensors, catalysts, and energy storage electrodes.

2. Experimental section

2. 1. Materials and methods

N-[3-(trimethoxysilyl) propyl]diethylenetriamine (the silane monomer used to prepare the SSG) was received from Sigma-Aldrich. $K_3[Fe(CN)_6]$, $CoCl_2$, and N_2H_4 were obtained from Dae-Jung Chemicals. All the chemicals were of analytical grade and were used as received. Field emission scanning electron microscopy (SEM) images were recorded using a JEOL JSM-7800F instrument. X-ray diffraction (XRD) profiles were recorded using a SmartLab (Rigaku) instrument. X-ray photoelectron spectroscopy (XPS) spectra were recorded using an ULVAC-PHI 5000 Versa Probe instrument. ITO (dimension: 2 × 1 cm^2) and its modified forms were used as a working electrode. A Pt wire served as a counter electrode, and Ag/AgCl (in 3 M NaCl solution) was used as a reference electrode. All the electrochemical experiments were conducted in a single-compartment three-electrode cell using an Ivium Technologies electrochemical work station. Nitrogen gas (N_2) was bubbled for 30 min before each experiment.

2.2 Synthesis of SSG solution

A homogeneous SSG solution was prepared [25] by adding 5 μL of 1 M silane monomer to 5 mL of aqueous solution under vigorous stirring, and the stirring was continued for another 60 min.

2.3 Fabrication of ITO/SSG-Cohcf electrode

A known volume (50 μL) of SSG solution was drop-cast on an ITO electrode that had been pre-treated with piranha solution (3:1, H_2SO_4:H_2O_2; *extreme care should be taken while handling*) and dried at 37°C. The dried ITO/SSG electrode was soaked in an acidic solution (0.01 M HCl) of 0.001 M $[Fe(CN)_6]^{3-}$ ions for 30 min, taken out, and rinsed in double-distilled water. Next, it was soaked in a solution containing Co^{2+} ions (0.001 M) for another 30 min, taken out, rinsed in double-distilled water, and allowed to dry. The process is illustrated schemati-

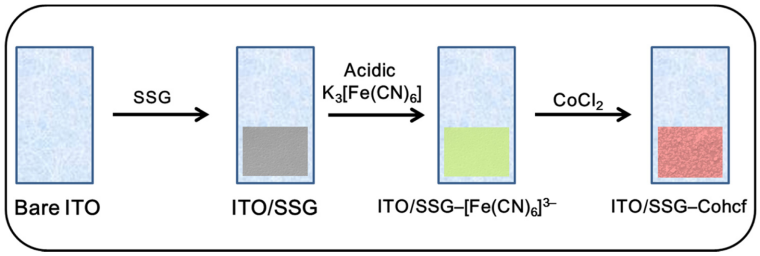

Fig. 1. Schematic representation of SSG-Cohcf electrode fabrication.

cally in Fig. 1.

2.4 Electrocatalysis and sensor

N_2H_4 electrooxidation at the ITO/SSG-Cohcf electrode was studied by recording cyclic voltammograms. During the measurements, 1 mM N_2H_4 was added to the electrolyte, which consisted of 0.1 M phosphate buffer solution (PBS) (pH 7.0). The experiments were performed at room temperature (25°C) in a potential window of -0.2 to 1.2 V. The N_2H_4 sensors were experimentally examined using linear sweep voltammograms (LSVs).

3. Results and Discussion

3.1 Surface characterization of the modified electrode

The surface modification process offers a platform to alter the basic structure of underlying substrates; therefore, the physical and chemical properties of materials can be tuned for use as electrodes with applications in sensing and catalysis. Fig. 2A-F illustrates that a stable electroactive Cohcf thin film was successfully fabricated by electrostatic adsorption of Co^{2+} on the ITO/SSG electrode pre adsorbed with $[Fe(CN)_6]^{3-}$ ions as an *in situ* chemical precipitant. The morphology of the Cohcf NSs shown in Fig. 2F demonstrates that the NSs are highly porous and interconnected. In addition, Cohcf is a polynuclear mixed-valence coordination compound, and its stoichiometry may vary depending on the preparation methodology, which could affect its electrochemical behavior. Fig. 2G-I summarizes the SEM-energy-dis-

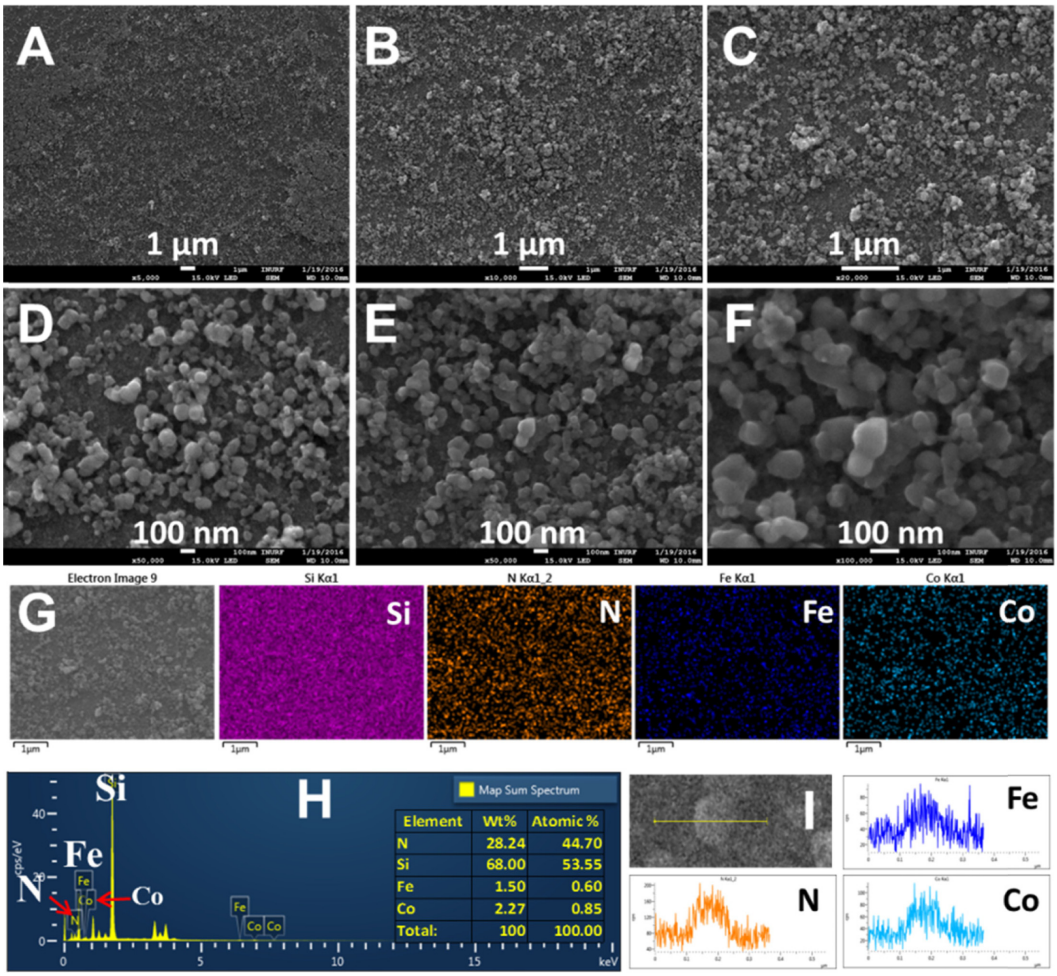

Fig. 2. (A-F) SEM images and (**G-I**) EDX analysis of SSG-Cohcf electrode.

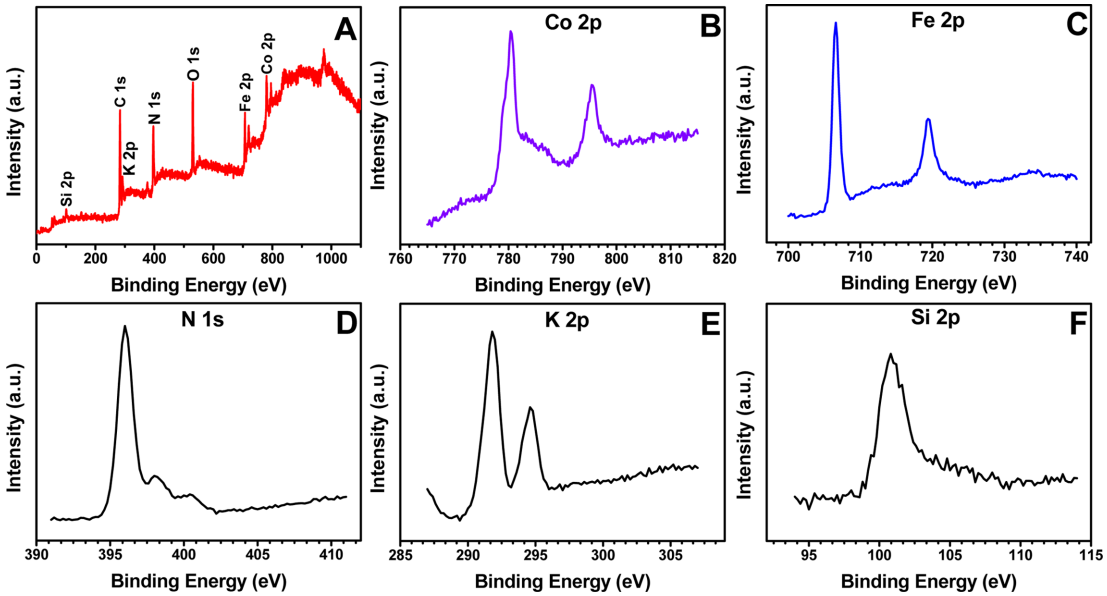

Fig. 3. XPS analysis of the ITO/SSG-Cohcf electrode.

persive X-ray (EDX) analysis of the ITO/SSG-Cohcf electrode and confirms the elemental composition and successful fabrication of Cohcf NSs by the electroless method. Furthermore, XRD (Fig. S1) and XPS (Fig. 3) analyses were performed to determine the crystallinity and identify the chemical components, respectively. As can be seen in Fig. S1, the peaks at 26.9, 35.7, 38.9, 53.8, and 56.2° were assigned to the (2 2 0), (4 0 0), (4 2 0), (6 0 0), and (6 2 0) planes, respectively, of the face-centered cubic Cohcf crystallographic structures [26]. As shown in Fig. 3, the core-level high-resolution scan mode revealed three metal ions (Co, Fe, and K) and two elements (N and Si). In addition, it can be inferred that Cohcf was interconnected and stabilized by the SSG.

The Cohcf NSs were successfully grown *in situ* at the ITO/SSG electrode via the electrostatic interaction between the irreversibly adsorbed $[Fe(CN)_6]^{3-}$ and Co^{2+} ions. Furthermore, the Cohcf NSs ranged in size from 100 to 200 nm (Fig. 2F) and were found to be densely packed throughout the ITO/SSG electrode, indicating a high amount Cohcf NS loading on the electrode surface. In the present approach, the amine groups of the SSG essentially served as nucleation sites [27] for the growth of Cohcf NSs. In addition, the highly porous 3D SSG acts as a host for accommodating the *in situ* grown Cohcf NSs. The electrostatic interaction between the positively charged SSG (due to the protonated NH_3^+) and the negatively charged $[Fe(CN)_6]^{3-}$ ions present in the acidic medium facilitates the irreversible adsorption of $[Fe(CN)_6]^{3-}$ ions at the ITO/SSG electrode [23]. The NH_2 groups of the SSG were protonated when the electrode was dipped in an acidic solution containing $[Fe(CN)_6]^{3-}$ ions. Next, the ITO/SSG-$[Fe(CN)_6]^{3-}$ electrode was dipped in a solution containing Co^{2+} ions, which led to *in situ* growth of Cohcf NSs at the SSG; the growth reached saturation within 30 min.

3.2 Growth and stability of the modified electrode

The electrochemical characteristics of Cohcf are well known, and it is widely assumed to be a suitable material for chemically modified electrodes for various applications. Fig. 4A shows the cyclic voltammogram of the modified electrode at a scan rate of 50 mV/s within a potential window of -0.2 to 1.2 V vs. a Ag/AgCl electrode. Two pronounced redox peaks are located at ~0.5 V. They correspond to the redox reaction of $Fe^{II/III}$ in Cohcf, which is accompanied by K^+ ions entering and exiting the cyano-bridged metallic framework to maintain local charge neutrality [28]. The symmetry of each peak indicates high reaction reversibility. Equation (1) describes the *in situ* growth of Cohcf NSs on the ITO/SSG elec-

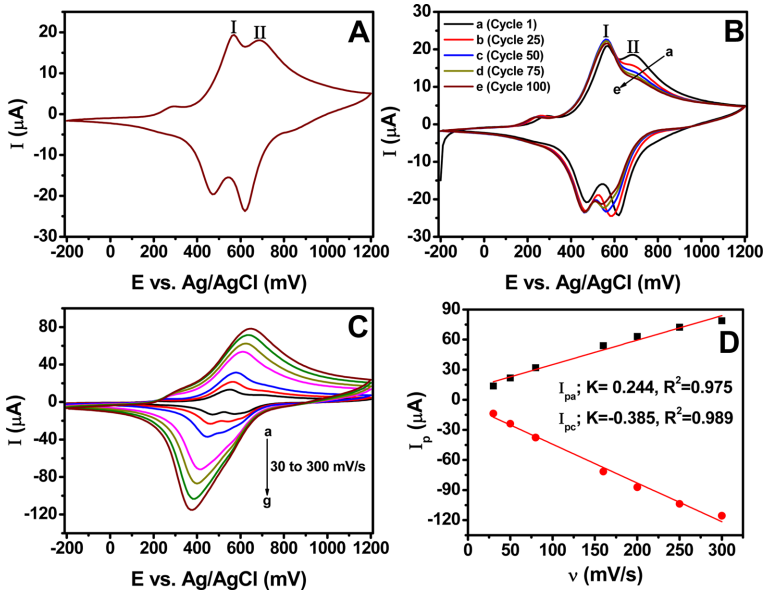

Fig. 4. (A, B) CV curves of ITO/SSG-Cohcf electrode in 0.1 M KCl obtained at a scan rate of 50 mV/s. (**A**) Cycle 1 and (**B**) (a-e) cycles 1-100 at intervals of 25 cycles, from outside to inside). **(C)** CV curves and (**D**) corresponding calibration plots of ITO/SSG-Cohcf electrode in 0.1 M KCl at various scan rates (30, 50, 80, 160, 200, 250, and 300 mV/s, from inside to outside).

trode during the electrostatic interaction between the irreversibly adsorbed $[Fe(CN)_6]^{3-}$ and Co^{2+} ions. Cohcf can exhibit two different stoichiometric forms [15] [Eqs. (2) and (3)]; hence, in its solid state, it can accept K^+ ions from the electrolyte to maintain electrical neutrality. This tendency toward K^+ ion insertion led to the appearance of the two redox peaks for the Cohcf NSs (Peak I: $Co_{1.5}^{(II)}[Fe^{(III)}(CN)_6]$ and Peak II: $KCo^{(II)}[Fe^{(III)}(CN)_6]$).

$$2.5\ CoCl_2 + 2\ K_3[Fe^{(III)}(CN)_6] \rightarrow Co_{1.5}^{(II)}[Fe^{(III)}(CN)_6] + KCo^{(II)}[Fe^{(III)}(CN)_6] + 5\ KCl \quad (1)$$

$$KCo_{1.5}^{(II)}[Fe^{(II)}(CN)_6] \leftrightarrow Co_{1.5}^{(II)}[Fe^{(III)}(CN)_6] + K^+ + e^- \quad (2)$$

$$K_2Co^{(II)}[Fe^{(II)}(CN)_6] \leftrightarrow KCo^{(II)}[Fe^{(III)}(CN)_6] + K^+ + e^- \quad (3)$$

Furthermore, the operational stability of the modified electrode is observed by recording 100 potential cyclic voltammetry (CV) cycles at a scan rate of 50 mV/s (Fig. 4B). Clearly, the current of peak I remains almost the same, whereas peak II exhibits a considerable current decrease in the forward scan and a negative shift in the backward scan. This finding can be explained as follows: the SSG offers good protection in terms of encapsulating the Cohcf NSs, and, during the potential CV cycles, insertion of K^+ ions leads to this typical redox behavior of peak II. To apply this material in device fabrication, good performance stability is the key factor to obtaining the desired efficiency; thus, the cycling stability of the modified electrode was examined by repetitive potential CV cycling. After 100 potential cycles, 92% of the original peak current (peak I) was retained, demonstrating the high chemical and structural robustness of the Cohcf NSs on the modified electrode. This improved operational stability, combined with the ease of preparation, makes it a highly promising candidate for device fabrication.

The effect of the scan rate (ν) on the peak currents (i_{pa} and i_{pc}) was investigated in the range of 30-300 mV/s (Fig. 4C). As the scan rate increased, two anodic and cathodic peaks merged completely, and the peak-to-peak separation of the redox pairs tended to increase, suggesting a limitation in the charge-transfer kinetics. In addition, the overlap between the two oxidative and reductive peaks was probably due to chemical interactions between the electrolyte spe-

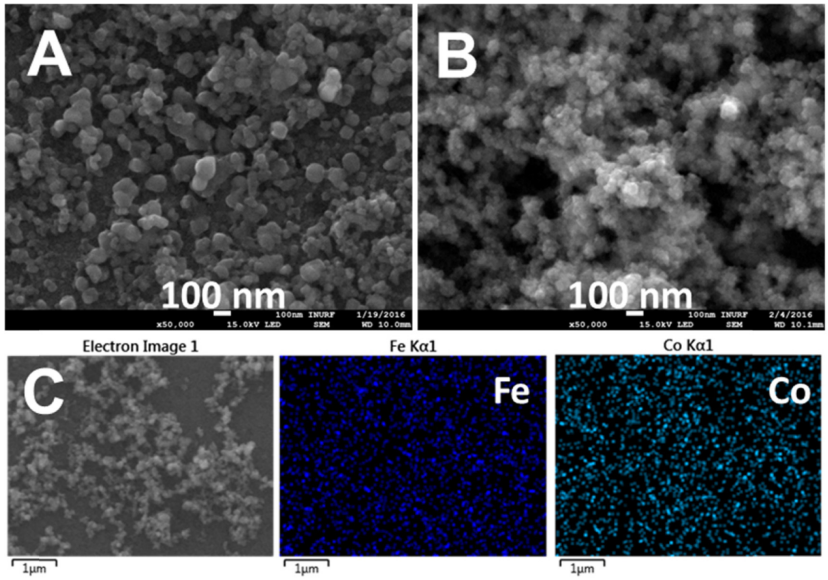

Fig. 5. (A,B) SEM images and (**C**) EDX analysis of SSG-Cohcf electrode (**A**) before and (**B,C**) after 100 potential CV cycles.

cies with cobalt ions at higher scan rates. The corresponding calibration plots (Fig. 4D) between the peak currents and the scan rates (v) for the redox reactions are linear. This observation clearly suggests that Cohcf NSs on the modified electrode, which nucleated throughout the 3D SSG and grew in the pores of the SSG, became SSG-encapsulated and interconnected. In addition, Cohcf NSs acted as charge transport carriers between the substrate and the solution interface.

Fig. 5A and B compares the SEM images before and after 100 potential CV cycles; structural deformation due to the insertion of K^+ ions from the electrolyte into the Cohcf NSs is clearly visible. The SEM-EDX analysis confirms the elemental composition after 100 CV cycles. Furthermore, from the cyclic voltammogram presented in Fig. 4A, the concentration of Cohcf NSs at the electrode surface (**Γ**) was calculated using Eq. (4) [23]:

$$\mathbf{\Gamma} = Q/(nFA) \quad (4)$$

where Q is the charge equivalent to the reduction peak (around 0.5 V), n is the number of electrons involved in the redox process, F is the Faraday constant, and A is the electrode area. The surface concentration of incorporated Cohcf was calculated as 2.0314×10^{-8} mol/cm^2. This larger surface coverage can provide more electrocatalytic sites.

3.3 Electrooxidation of N_2H_4

N_2H_4 is a precise analyte that has high oxidation overpotential; hence, it cannot be oxidized on bare electrodes. In this study, we investigated the electrochemical features of N_2H_4 on the fabricated modified electrodes and the bare electrode (see summary in Figs. 6-8). Fig. 6A shows the CV curves of the Cohcf-NS-modified electrodes in 0.1 M PBS (pH 7.0) in the absence (a) and in the presence (b) of N_2H_4. A comparison of these two CV curves indicates the vital role of Cohcf NSs in the film, i.e., electrochemically generation (at 0.52 V) upon oxidation of N_2H_4. An increase of ca. 23.10 μA in the current in the anodic region corresponding to oxidation of Fe^{II} to Fe^{III} (first peak at 0.52 V) on the ITO/SSG-Cohcf electrodes is observed when N_2H_4 is added. The increased current response due to the addition of N_2H_4 in the anodic region can be attributed to diffusion of N_2H_4 toward the electrode surface, and the current electrochemically reduces the produced Fe^{III}. In addition, the Fe^{II} is regenerated by N_2H_4 during the potential sweep; consequently, the anodic current increases. As shown in Fig. 6B, the electrochemical responses toward N_2H_4 are almost negligible on bare

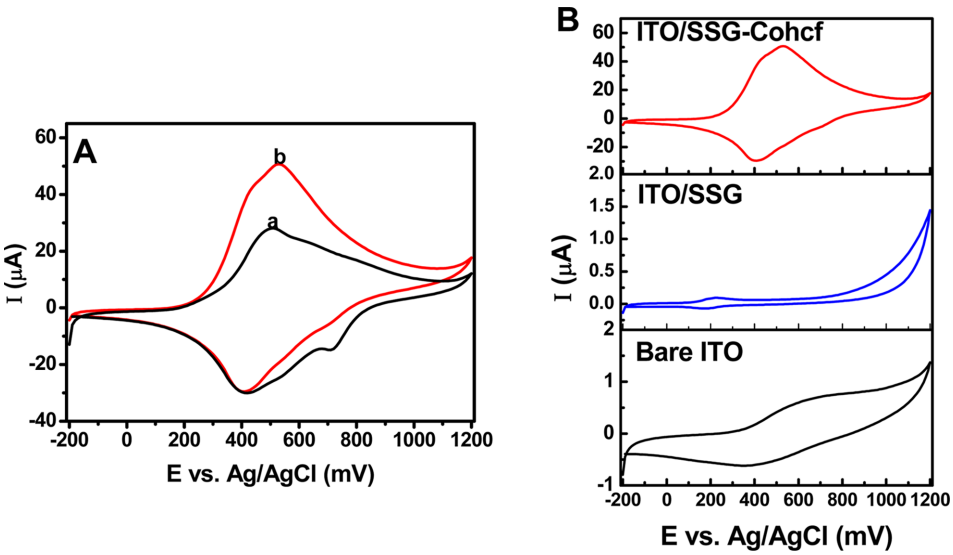

Fig. 6. (**A**) Comparison of CV curves at ITO/SSG-Cohcf electrode in the (a) absence and (b) presence of 1 mM N_2H_4. (**B**) CV curves obtained on bare ITO, ITO/SSG, and ITO/SSG-Cohcf electrodes in the presence of 1 mM N_2H_4. Conditions: supporting electrolyte, 0.1 M PBS (pH 7.0); scan rate, 50 mV/s.

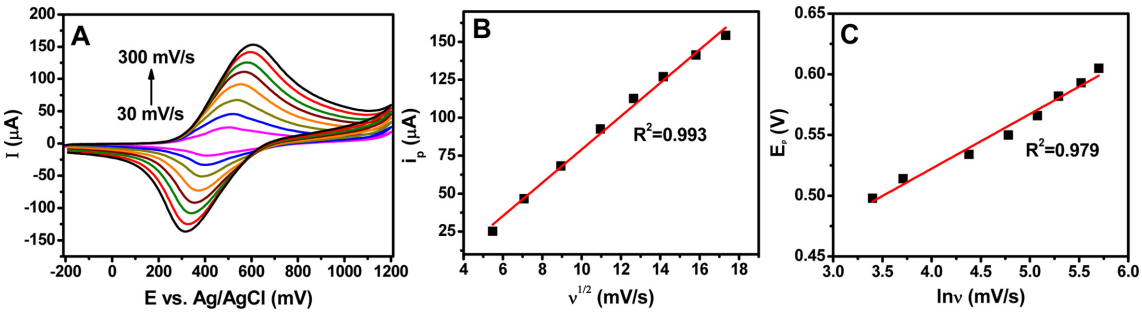

Fig. 7. (**A**) Electrochemical response of ITO/SSG-Cohcf electrode to 1 mM N_2H_4 at scan rates of 30, 50, 80, 120, 160, 200, 250, and 300 mV/s. (**B**) Peak current as a function of the square root of the scan rate, and (**C**) linear relationship of peak potential against the natural logarithm of the scan rate.

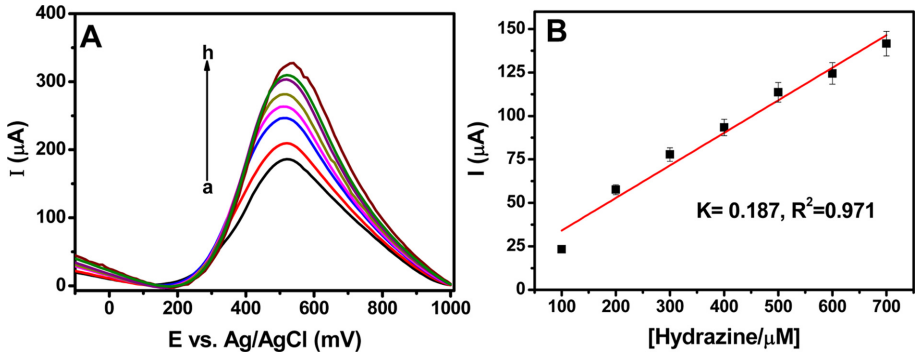

Fig. 8. (**A**) LSVs recorded on the ITO/SSG-Cohcf electrode in 0.1 M PBS (pH 7.0) for (a) no N_2H_4 and (b) 100 μM, (c) 200 μM, (d) 300 μM, (e) 400 μM, (f) 500 μM, (g) 600 μM, and (h) 700 μM N_2H_4. (**B**) Corresponding calibration plot.

ITO (a) and ITO/SSG (b) electrodes. In contrast, a well-behaved anodic wave formed at a peak potential of 0.52 V on the ITO/SSG-Cohcf electrode (Fig. 6A). In addition, in the absence of the Cohcf NSs, N_2H_4 was oxidized around 0.8-0.9 V on the bare ITO and ITO/SSG electrodes, whereas a large decrease in the overpotential can be observed on the ITO/SSG-Cohcf electrode. This distinct electrochemical response ("b" in Fig. 6A) at the reduced overpotential for N_2H_4 is facilitated by the highly porous and interconnected Cohcf NSs on the modified electrode. We further investigated the electrochemical features of N_2H_4 on the ITO/SSG-Cohcf electrode by recording CV curves at various scan rates (30-300 mV/s) (Fig. 7). With increasing scan rate, the oxidation peak potential shifted in the positive direction, and the oxidation current was also enhanced. A plot of the anodic peak current versus the square root of the scan rate ($v^{1/2}$) shows a linear relationship, revealing a diffusion-controlled process [29]. In addition, the peak potential was directly proportional to the natural logarithm of the scan rate (ln v), revealing a kinetic limitation in the reactions between the redox sites of the electron transfer mediator (Cohcf) and N_2H_4 [30]. LSVs were obtained for the ITO/SSG-Cohcf electrode by adding 100 μM N_2H_4; the results are summarized in Fig. 8. At the sensor electrode, the Cohcf NSs exhibited a stable response, and the catalytic current was proportional to the concentration of N_2H_4. A linear dependence of the oxidation peak current due to N_2H_4 addition was obtained with a correlation coefficient (R^2) of 0.971, and the sensitivity was 0.187 μA/μM.

4. Conclusions

In summary, a facile approach was successfully developed for *in situ* growth of Cohcf NSs on an electrode surface via electrostatic interaction. Their structural features facilitate the passage of charge-balancing ions from the electrolyte (K^+) in and out of the framework and thus advance the electrochemical redox reaction of Cohcf. Owing to its chemical and structural stability, an ITO/SSG-Cohcf electrode exhibited impressive potential cycling stability. Given the ease of preparation and cost-effectiveness, Cohcf and other Prussian blue analogs may hold great promise for future energy storage applications. We further analyzed the electrochemical behavior and electrocatalytic ability of the modified electrode toward N_2H_4. Electrooxidation of N_2H_4 was observed at a reduced overpotential and was attributed to the synergistic catalytic effect resulting from the combination of Cohcf and the SSG. Linear sweep voltammetry was used to quantify the amount of N_2H_4. This method of fabricating Cohcf NSs has great relevance to the preparation of films that may find applications in enzymeless biosensors, fuel cells, future photomagnetic devices, and energy systems.

Acknowledgments

This research was supported by Post-Doctor Research Program(2015) through Incheon National University(INU), Incheon, Republic of Korea.

Supporting Information

XRD analysis of SSG-Cohcf electrode

References

[1] S. Q. Liu and H. Y. Chen, *Journal of Electroanalytical Chemistry*, **2002**, *528*, 190-195.
[2] M. H. Pournaghi-Azar and H. Dastangoo, *Journal of Electroanalytical Chemistry*, **2002**, *523(1)*, 26-33.
[3] P. Wang, X. Jing, W. Zhang and G. Zhu, *Journal of Solid State Electrochemistry*, **2001**, *5(6)*, 369-374.
[4] X. Cui, L. Hong and X. Lin, *Journal of Electroanalytical Chemistry*, **2002**, *526(1)*, 115-124.
[5] A. M. Vinu Mohan, G. Rambabu, K. K. Aswini and V. M. Biju, *Thin Solid Films*, **2014,** *565*, 207-214.
[6] S. M. Chen, *Electrochimica Acta*, **1998,** *43(21),* 3359-3369.
[7] K. Deng, C. Li, X. Qiu, J. Zhou and Z. Hou, *Electrochimica Acta*, **2015,** *174*, 1096-1103.
[8] X. Luo, J. Pan, K. Pan, Y. Yu, A. Zhong, S. Wei, J. Li, J. Shi and X. Li, *Journal of Electroanalytical Chemistry*, **2015,** *745,* 80-87.
[9] F. Zhao, Y. Wang, X. Xu, Y. Liu, R. Song, G. Lu and Y. Li, *ACS Applied Materials and Interfaces*, **2014,** *6(14),* 11007-11012.
[10] C. D. Wessells, R. A. Huggins and Y. Cui, *Nature Communications*, **2011,** *2*, 550.
[11] P. J. Kulesza, M. A. Malik, A. K. Miecznikowski, A. Wolkiewicz, S. Zamponi, M. Berrettoni and R. Marassi, *Journal of the Electrochemical Society*, **1996**, *143(1)*, L10-L12.
[12] A. Bleuzen, C. Lomenech, V. Escax, F. Villain, F. Varret, C. Cartier Dit Moulin and M. Verdaguer, *Journal of the American Chemical Society*, 2000, **122(28)**, 6648-6652.
[13] C. Cartier Dit Moulin, F. Villain, A. Bleuzen, M. A. Arrio, P. Sainctavit, C. Lomenech, V. Escax, F.

Baudelet, E. Dartyge, J. J. Gallet and M. Verdaguer, *Journal of the American Chemical Society*, **2000**, *122(28)*, 6653-6658**.**

[14] A. Eftekhari, *Mikrochimica Acta*, **2003,** *141(1-2)*, 15-21.

[15] S. Thangavel and R. Ramaraj, *Journal of Nanoscience and Nanotechnology*, **2009,** *9(4),* 2353-2363.

[16] J. Du, Y. Wang, X. Zhou, Z. Xue, X. Liu, K. Sun and X. Lu, *Journal of Physical Chemistry C*, **2010**, *114(35),* 14786-14793.

[17] F. N. Crespilho, V. Zucolotto, C. M. A. Brett, O. N. Oliveira Jr and F. C. Nart, *Journal of Physical Chemistry B*, **2006**, *110(35),* 17478-17483.

[18] A. Ahmadalinezhad, A. K. M. Kafi and A. Chen, *Electrochemistry Communications*, **2009,** *11(10),* 2048-2051.

[19] G. Chang, Y. Luo, W. Lu, J. Hu, F. Liao and X. Sun, *Thin Solid Films*, **2011,** *519(18),* 6130-6134.

[20] Q. Yi, F. Niu and W. Yu, *Thin Solid Films*, **2011,** *519(10), 3*155-3161.

[21] S. Durga, K. Ponmani1, S. Kiruthika, B. Muthukumaran, *J. Electrochem. Sci. Technol*, **2014**, *5(3)*, 73-81.

[22] S. Amlathe and V. K. Gupta, *Analyst*, **1988,** *113(9),* 1481-1483.

[23] S. Manivannan, I. Kang and K. Kim, *Langmuir*, **2016***, 32(7)*, 1890-1898.

[24] S. Manivannan and R. Ramaraj, *Journal of Nanoparticle Research*, **2012,** *14(6)*, 1-11.

[25] S. Manivannan and K. Kim, *Journal of Electroanalytical Chemistry*, **2016**, *776,* 82-92.

[26] S. Choudhury, G. K. Dey and J. V. Yakhmi, *Journal of Crystal Growth*, **2003,** *258(1)*, 197-203.

[27] S. Manivannan and R. Ramaraj, *Journal of nanoparticle research*, **2013**, *15(10)*, 1-13.

[28] F. Zhao, Y. Wang, X. Xu, Y. Liu, R. Song, G. Lu and Y. Li, *ACS Applied Materials & Interfaces*, **2014**, *6(14),* 11007-11012.

[29] H. Heli, I. Eskandari, N. Sattarahmady and A. A. Moosavi-Movahedi, *Electrochimica Acta*, **2012,** *77,* 294-301.

[30] A. Naeemy, Journal of Electrochemical Science and Technology, **2015,** *6(3),* 88-94.